

A Coherent Interpretation of the Form Factors of the Nucleon in Terms of a Pion Cloud and Constituent Quarks

J. Friedrich and Th. Walcher

Institut für Kernphysik, Universität Mainz, D-55099 Mainz

Received: date / Revised version: date

Abstract. The recent unbiased measurements of the electric form factor of the neutron suggest that its shape may be interpreted as a smooth broad distribution with a bump at $Q^2 \approx 0.3$ (GeV/c)² superimposed. As a consequence the corresponding charge distribution in the Breit frame shows a negative charge extending as far out as 2 fm. It is natural to identify this charge with the pion cloud. This realisation is then used to reanalyse all old and new data of the electric and magnetic form factors of the proton and the neutron by a phenomenological fit and by a fit based on the constituent quark model. It is shown that it is possible to fit all form factors coherently with both ansaetzen and that they all show the signal of the pion cloud.

PACS. 14.20.Dh – 13.40.Gp – 21.10.Ft

1 Introduction

Form factors encode unique information about the internal structure of a scatterer provided they are determined with sufficient precision over a sufficiently large range of momentum transfer. Depending on the interaction, the Fourier transformation of the form factors gives the spatial distribution of e.g. mass, charge or magnetisation, which provides insight into several aspects of the internal structure of the scatterer:

- the constituents present in the system,
- their interaction,
- and their wave functions.

Therefore, form factors represent very significant tests of any model of the scatterer.

The nucleon is realized in nature in two species, the proton with one charge unit and the neutron with no net charge. While the proton should dominantly be describable by the s-state wave functions of the two up and the one down constituent quark, these contributions cancel to first order in the neutron and its electric form factor should be zero in this approximation. In this simple picture it is assumed that the quarks are dressed by gluons and sea quarks forming “constituent quarks” which represent effective Fermions with equal masses of about one third of the nucleon mass. However, already before the realization of the quark-gluon structure of the nucleon the perception of a pion cloud around the nucleon was used in order to account for the Yukawa interaction between the nucleons. After early pure quark models of the nucleon, like the MIT bag, the necessity of a pion cloud was soon realized in order to preserve chiral symmetry at the nucleon surface, and the “little bag” and “cloudy bag” models were invented. Based on the fundamental chiral symmetry of the QCD Lagrangian “chiral dynamics” was developed identifying the pion as the almost Goldstone

Boson of the strong interaction. The “chiral perturbation theory” based on it has shown through many experimental tests that indeed the pion is a decisive constituent of the nucleon besides the elementary quarks and gluons. It is the purpose of this paper to check whether and how the pion cloud is reflected in the nucleon form factors.

Because of its zero charge, the contribution of the bare neutron n^0 to the electric form factor of the physical neutron n is small, and the dissociation of a nucleon into its counterpart (here: the proton), and a charged pion (here: a negative pion) should emerge most clearly in the neutron’s electric form factor G_{En} . We therefore start out in section 2 with a discussion of G_{En} for which now unbiased data exist from polarisation measurements [1–14]. In section 3 we give an overview of the existing relevant form factor measurements and of our data selection for the present investigation. In section 4 we show that, at the percentage level, the peculiar structure observed in G_{En} , namely a kind of bump around $Q^2 \approx 0.2 - 0.3$ (GeV/c)², is also present in the other form factors G_{Ep} , G_{Mp} , and G_{Mn} . While this is discussed in section 4 in terms of a purely phenomenological ansatz for the form factors, we show in section 5 how this can be viewed in the light of the decomposition of the nucleon states into a constituent quark core and a polarisation term reflecting the contribution of the pion cloud. The findings are discussed in the concluding section 6.

2 The triggering conjecture: The electric form factor of the neutron G_{En}

Previous efforts to determine the electric form factor of the neutron, e. g. from elastic electron scattering on the deuteron, were hampered by severe model-dependencies of the results,

which therefore were uncertain to about 50%. The emerging results were describable by the so called Galster parameterisation, which started out from the usual dipole fit, which reproduced G_{Ep} , G_{Mp} , and G_{Mn} reasonably well and which was multiplied by some appropriate function in order to account for the condition $G_{En}(Q^2 = 0) = 0$ required by the vanishing charge of the neutron. This Galster form is given by

$$G_{En}(Q^2) = \frac{a_G \tau}{(1 + b_G \tau)} \cdot \frac{1}{(1 + Q^2/m_D^2)^2}, \quad (1)$$

where $\tau = Q^2/(2m_n)^2$ and $m_n = 0.939 \text{ GeV}/c^2$ is the neutron mass. The parameter m_D^2 was taken as the standard dipole value $m_D^2 = 0.71 \text{ (GeV}/c)^2$ and $a_G = 1.73$ in order to reproduce the measured root mean square radius of the neutron of $\langle r^2 \rangle = -6 dG_{En}(Q^2)/dQ^2|_{Q^2=0} = -0.115 \text{ fm}^2$ as determined from the scattering of thermal neutrons [15]. Thus the only parameter free to be fitted to the data was b_G , and it was determined to $b_G = 4.62$. The Galster form has no particular theoretical justification and may rather hide the essential physics.

The collected data for G_{En} determined recently from polarisation measurements are depicted in fig. 1. These 15 data

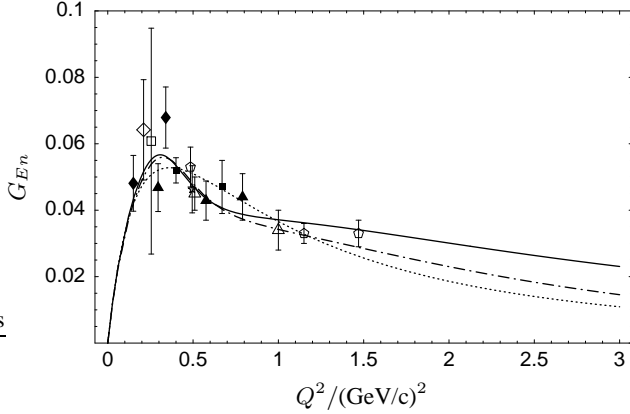


Fig. 1. The G_{En} data from polarisation measurements. The coding for reactions with the deuteron as a neutron target is: open square [1], filled diamonds [2, 3], open diamond [4], open star [9], open triangle [14], open pentagon [12, 13], and filled triangle [10, 11], the measurements with ${}^3\text{He}$ are shown as filled squares [5–8]. The full curve depicts the fit of the parameters of eq. (2) to the data, the dashed dotted curve is a variant with slightly changed parameters as explained in the text, while the dotted curve is a fit using the Galster form, i.e. eq. (1).

points, which are not hampered by model assumptions, have been taken with 8 very different experimental setups, and the data points taken with the same setups were taken over periods separated by long time intervals. Also, the setups had very different systematic errors and corrections due to nuclear binding effects. Therefore, it is justified to consider the data as statistically independent. Since the corrections are less certain for the measurements on ${}^3\text{He}$ than for the loosely bound deuterium, the measurements on the two targets are distinguished in fig. 1 by markedly different symbols. It is not the aim of this paper, however, to discuss critically these experiments but just to take this data set seriously and to investigate its essential features.

It is evident from fig. 1 that the data can be as well regarded as a broad distribution and a peak around $Q^2 \approx 0.3 \text{ (GeV}/c)^2$ not present in the smoother Galster fit.

In order to get some insight into the consequences of this alternative form we have added a term to the form of eq. (1) which is able to describe an additional peak with reasonable boundary conditions.

$$G_{En}(Q^2) = \frac{a Q^2}{(1 + b Q^2 + c Q^{10})} + \frac{d Q^2}{(1 + e Q^2)(1 + f Q^2)^2}. \quad (2)$$

The rms radius is now given by the sum of a and d , constrained to $(a + d)(2m_n)^2 = a_G = 1.73$, and we fixed a and d to $a = 0.37 \text{ (GeV}/c)^{-2}$ and $d = 0.12 \text{ (GeV}/c)^{-2}$. The parameters e and f were kept fixed at $0.5 \text{ (GeV}/c)^{-2}$. Minimising χ^2 yielded $b = 6.02 \text{ (GeV}/c)^{-2}$ and $c = 229 \text{ (GeV}/c)^{-10}$. Here we only want to have a parametrisation which reproduces the data within the experimental error bars without associating any particular physical meaning with the single parameters. In fact, as seen in fig. 1, this form reproduces the data well. It is not meaningful to go into any detail of an error analysis, instead we only show by the example of the dashed-dotted curve that with above parametrisation the “peak-region” and the tail to higher momentum transfers are essentially described independently from each other. For completeness we just mention that the χ^2 of the Galster form is by about $\Delta\chi^2 = 4.8$ bigger than that of the two others.

As is well known [16], though sometimes questioned (for a discussion of this problem see ref. [17]), the Fourier transform of the electric and magnetic Sachs form factors $G_E(Q^2)$ and $G_M(Q^2)$ represent the charge and magnetic density distribution in the Breit frame, where the energy transfer $\omega = 0$ and the three-momentum transfer $|\mathbf{q}_{\text{Breit}}| = Q$; we denote these distributions by $\rho(r)$, which thus is given by

$$\rho(r) = \frac{4\pi}{(2\pi)^3} \int_0^\infty G(Q) \frac{\sin(Qr)}{Qr} Q^2 dQ. \quad (3)$$

Refinements to this relation are discussed in detail in ref. [18] where it is also pointed out that corrections cannot be defined without model assumptions. Since we are interested in the gross features of the measured form factors and the spatial distributions, we base our further discussion on eq. (3). A more refined approach may result in some compression of the resulting distributions in r-space, which should not alter their salient features and which are therefore left out of consideration in this paper.

Fig. 2 shows the charge distribution in the neutron, ρ_{En} , calculated via eq. (3) with above given fits to G_{En} . We have plotted $r^2 \rho_{En}(r)$ which represents the charge in a spherical shell at radius r . The charge distribution of the Galster fit shows the well known “aperiodic” shape with a positive bump in the interior and a negative bump at the outside of the neutron. This characteristic feature also results from an ansatz for the form factor with the superposition of two appropriate dipole forms, to which the Galster parameterisation is a good approximation.

The fit with eq. (2), however, which accounts for the bump in G_{En} at $Q^2 \approx 0.3 \text{ (GeV}/c)^2$, results in an oscillatory behaviour of $\rho_{En}(r)$ (see fig. 2). Though the oscillatory behaviour

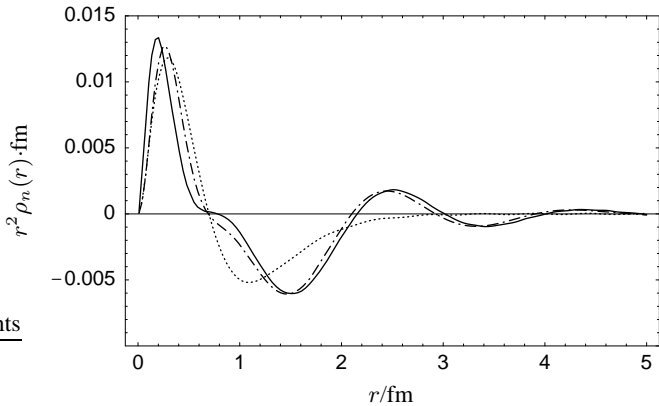


Fig. 2. The differential radial charge distribution of the neutron in the Breit frame as derived by a Fourier transform. The coding of the lines is that of fig. 1.

depends on the particular fitting form we shall show that it is the bump which shifts more charge to the outside than does the Galster fit. Since this outer region should be dominated by the pion cloud, the corresponding contribution should show up as a general feature also in the other form factors, where, however, a form factor bump of the same order of magnitude can only be expected to be a few-percent contribution.

With this in mind, we reconsider all four nucleon form factors in the following.

3 The data base

Table 1 gives an overview of the data which we have taken into consideration together with the Q^2 -ranges which they cover.

For G_{Ep} we have omitted in the final analysis the data by Andivahis et al. [22]. In the Q^2 -range of these data, $G_{Ep} \ll G_{Mp}$, thus its determination via a Rosenbluth separation is quite uncertain. In fact these data are clearly incompatible with the new results from polarisation measurements in which not the sum of $G_{Ep}^2 + \tau \cdot G_{Mp}^2$ is measured but the ratio G_{Ep}/G_{Mp} . It is straightforward to determine G_{Ep} from this ratio if one takes the prevailing G_{Mp} as known from measurement.

For G_{Mp} we took into account the same data as Kelly [18], i. e. the data by Hoehler et al. [29] up to $Q^2 = 0.15$ (GeV/c) 2 and those revised and compiled recently by Brash et al. [45]. In addition we also used the data by Hanson et al. [23].

For G_{En} we have only taken into account the data from polarisation measurements. The measurement in [35, 23] give only G_{En}^2 , thus the sign of G_{En} remains undetermined, and the errors are so large that the data can essentially be regarded as upper limits only; we did not take them into account in the fits. Other determinations of G_{En} were very uncertain due to the model dependency of the extraction of G_{En} from the measured cross sections, and we did not take them into consideration.

For G_{Mn} the data by Markowitz et al. [39] and by Bruins et al. [40] were omitted in the analysis as was already done (and argued) in Kubon et al. [36]. Also, the data by Hanson et al. [23] are omitted since they deviate substantially from the trend of the more recent data measured with the detection of the neutron in coincidence.

Measurement	Q^2 -range	reference
G_{Ep} $p(e, e')$	0.01 - 0.05 0.04 - 1.75 0.39 - 1.95 (1.75 - 8.83)	Simon et al. [19] Price et al. [20] Berger et al. [21] Andivahis et al. [22]
$d(e, e'p)$ $p(\vec{e}, e' \vec{p})$	0.27 - 1.76 0.37 - 0.44 0.38 - 0.50 0.40 0.49 - 3.47 3.50 - 5.54	Hanson et al [23] Pospischil et al. [24] Milbrath et al. [25] Dieterich et al. [26] Jones et al. [27] Gayou et al. [28]
G_{Mp} $p(e, e')$	0.02 - 0.15 0.16 - 0.86 0.39 - 1.75 0.67 - 3.00 1.00 - 3.00 1.50 - 3.75 1.75 - 7.00 2.86 - 31.2 0.27 - 1.76	Hoehler et al. [29] Janssens et al. [30] Berger et al. [21] Bartel et al. [31] Walker et al. [32] Litt et al. [33] Andivahis et al. [22] Sill et al. [34] Hanson et al [23]
G_{En} $d(\vec{e}, e' \vec{n})p$	0.15 0.26 0.30, 0.58 0.34 0.49 - 1.47 0.76 1.00 $\vec{d}(\vec{e}, e' n)p$ 0.21 0.50 ${}^3He(\vec{e}, e' n)$ 0.40 0.67 $d(e, e')$ (0.27 - 1.76) (1.75 - 4.00)	Herberg et al. [3] Eden et al. [1] Seimetz et al. [10] Ostrick et al. [2] Madey et al. [12, 13] Glazier et al. [11] Day et al. [14] Passchier et al. [4] Zhu et al. [9] Becker et al. [6-8] Rohe et al. [5, 8] Hanson et al [23] Lung et al. [35]
G_{Mn} $d(e, e' n)p$	0.07 - 0.89 0.10 - 0.20 0.11 (0.11 - 0.26) (0.13 - 0.61) 0.24 - 0.78 $d(e, e' p)$ $d(e, e')$	Kubon et al. [36] Xu et al. [37] Anklin et al. [38] Markowitz et al. [39] Bruins et al. [40] Anklin et al. [43] Hanson et al [23] Lung et al. [35] Rock et al. [44]

Table 1. Overview of data taken into consideration (Q^2 in (GeV/c) 2). The data left out in the final analysis are put into parentheses. The reactions are as indicated; $d(e, e')$ refers to quasi elastic scattering.

4 A phenomenological description of the nucleon form factors

4.1 The phenomenological ansatz

What we are particularly interested in is the existence of a small bump on top of a large “smooth main part”. This raises the question after what is “smooth main part” and what is “bump”. After the investigation of several parameterisations we decided to keep close to what one is used to in the description of the nucleon form factors, namely the dipole form. In fact it is fascinating that the three form factors G_{Ep} , G_{Mp} , and G_{Mn} are describable to quite a precision by the dipole form with the one parameter m_D given above as it has entered into the text books, e. g. [16, 46]. Such good description could make one believe that there is some physical meaning in the parameter m_D . In fact there is none.

Looking at the form factors more closely, however, the precision with which the measurements are reproduced by this simple parameterisation is limited. While this has been realized on the percentage level already in the high-precision measurement of G_{Ep} at low Q^2 by Simon et al. [19], this became completely obvious at high Q^2 by the polarisation measurements by Jones et al. [27].

Purely phenomenologically, we describe the smooth part of the form factors, $G_s(Q^2)$, by the dipole form. In order to be somewhat flexible, however, we took into account the superposition of two dipoles:

$$G_s(Q^2) = \frac{a_{10}}{(1 + Q^2/a_{11})^2} + \frac{a_{20}}{(1 + Q^2/a_{21})^2}. \quad (4)$$

To account for a possible bump on top of the smooth form factor we now take a parameterisation which is easy to handle and the parameters of which give direct insight into the characteristic features of such a bump, namely its amplitude, position and width, a_b , Q_b , and σ_b , respectively. A quite natural choice would be a Gaussian positioned at Q_b . For $Q_b \neq 0$, however, such Gaussian contains uneven powers in Q , which is not allowed for a function representing a form factor. This shortcoming can be healed by superimposing two Gaussians as introduced in r-space by Sick for his ansatz for a model-independent analysis of nuclear charge distributions [47]. We thus parameterise the bump as

$$G_b(Q^2) = e^{-\frac{1}{2}(\frac{Q-Q_b}{\sigma_b})^2} + e^{-\frac{1}{2}(\frac{Q+Q_b}{\sigma_b})^2}. \quad (5)$$

In order to keep as close as possible to the accustomed description of the form factors, we attribute the full normalisation to the dominating smooth part, i. e. $G_N(Q^2 = 0) = G_s(Q^2 = 0)$, i. e. in this ansatz the smooth part accounts for the full charge or magnetic moment, respectively. To make sure, that, independent of the fitted values for its parameters, G_b does not interfere with this normalisation, we multiply it by Q^2 . We thus parameterise the nucleon form factors by the ansatz

$$G_N(Q^2) = G_s(Q^2) + a_b \cdot Q^2 G_b(Q^2), \quad (6)$$

where a_b is essentially the amplitude of the bump.

4.2 Fit of the form factors with the phenomenological ansatz

The parameters from the fits of above phenomenological ansatz to the form factors G_{Ep} , G_{Mp} , G_{En} , and G_{Mn} are compiled in table 2. The given errors are the standard errors from the fit procedure, which also account for correlations, therefore the parameters cannot just be varied independently within these margins.

The main purpose of these fits is to allow a coherent view on the measured form factors in order to reveal certain common features. Therefore we do not go into details of these fits - let alone the hundreds of other fits which we also tried. We only want to point to some particular features of these fits.

The final fitting results given here have been performed with fixed normalisation which was guaranteed by setting $a_{20} = 1 - a_{10}$ and fitting only a_{10} to the data ($a_{20} = -a_{10}$ for G_{En}). Fits with both a_{10} and a_{20} as free parameters did not improve the fits by more than $\Delta\chi^2 = -2$; this means that there is no hint for normalisation problems in the data.

Let us first look at the “standard form factors” G_{Ep} , G_{Mp} , and G_{Mn} , which we refer to as G_N^{std} . For these, one dipole (the first) accounts for the overwhelming part of the strength at low q , i. e. it carries most of the charge or magnetisation, respectively. The slope constants of all three G_N^{std} essentially agree within the errors. In fact, the mean value $0.76 \text{ (GeV/c)}^{-2}$ is near to the value $m_D^2 = 0.71 \text{ (GeV/c)}^{-2}$ of the standard dipole fit, however the deviation is significant. In fact one cannot expect equal parameters since the standard dipole fit deviates systematically from the data (c.f. fig. 4) and thus also from our fits which reproduce the data within the experimental errors.

It is interesting to note, that also the slope parameters a_{21} of the second dipole form are very similar for all three G_N^{std} (cf. fit 1 for G_{Mp} in table 2). This term (with negative amplitude) accounts for the fact that the measurements fall below the dipole fit at larger Q^2 . While this became obvious for G_{Ep} at larger Q^2 from polarisation measurements, a systematic deviation from the dipole fit was already observed by Simon et al. [19] at low Q^2 , though only at the percent level. It may now be somewhat surprising that the slope parameters a_{21} are so similar for all three G_N^{std} . In fact, if one accounts in G_{Mp} also for the high Q region (fit 2), this is no longer the case.

A direct interpretation of the bump structure in terms of the parameters a_b , Q_b , and σ_b is obscured by the multiplication of the Gaussian with Q^2 . Therefore, for a discussion of this structure we refer to its graphical representation in fig. 5.

First, fig. 3 shows the overall behaviour of the nucleon form factors and the quality of the overall agreement with the fits. For G_{Ep} the relatively large (negative) amplitude a_{20} of the second dipole results in a zero in the form factor around $3 \text{ GeV}/c$. This makes this form factor look very differently from G_{Mp} and G_{Mn} , though, in fact, this is only due to the larger amplitude of the dipole with negative sign and not the form of the single contributions. At the highest measured momentum transfers above $3 \text{ GeV}/c$ the data for G_{Mp} are not so well described by this phenomenological fit. Though, from χ^2 , the overall description of the data is excellent, there might be some systematic deviation at high Q^2 pointing to insufficient flexibility of the ansatz.

form factor	G_s				G_b						
	a_{10}	a_{11} (GeV/c) ²	a_{20}	a_{21} (GeV/c) ²	a_b (GeV/c) ⁻²	Q_b (GeV/c)	σ_b (GeV/c)	$N_{d.f.}$	$\chi^2_{d.f.}$	χ^2_{total}	
G_{Ep}	1.041(40)	0.765(66)	-0.041(-)	6.2(5.0)	-0.009(7)	0.07(88)	0.27(29)	64	0.933	59.71	
G_{Mp}/μ_p 1 2	1.002(7)	0.749(6)	-0.002(-)	6.0(3.4)	-0.005(1)	0.35(7)	0.21(3)	60	0.861	51.66	
	1.003(7)	0.753(2)	-0.003(-)	16.9(6)	-0.006(2)	0.33(7)	0.23(3)	75	0.876	65.7	
G_{En}	1.78(40.0)	1.73(-)	-1.78(-)	1.62(2.64)	0.010(7)	0.25(19)	0.22(11)	10	0.954	9.54	
G_{Mn}/μ_n	1.012(6)	0.770(10)	-0.012(-)	6.8(3.0)	-0.011(1)	0.33(3)	0.14(2)	14	0.579	8.11	

Table 2. Parameters from the fit of the phenomenological ansatz eq. (6) to the electric and magnetic nuclear form factors. In the usual way the errors on the parameters are given in brackets; if no decimal point is given they refer to the last given digits of the parameter. For G_{Mp} , fit 1 uses only the data up to 2 GeV/c, thus it is more comparable to the fits to G_{Ep} and G_{Mn} than the fit 2 where all data up to 6 GeV/c are taken into account.

In order to make the deviation of the measurements (and thus also of our fits) from the standard dipole fit more obvious, we show in fig. 4 the ratio of the three standard form factors (data and fit) to the standard dipole fit (see second factor of eq. (1)).

In fig. 5 we demonstrate the “bump”-contribution to the form factors by the subtraction of the fitted smooth part, i. e. the two dipoles. In order to emphasise the low- Q^2 region where this phenomenon occurs, we have plotted this difference as function of $\log(Q^2)$. It is obvious from this graph that the bump structure around $Q^2 = 0.2 - 0.3$ (GeV/c)², as discussed in section 2 for G_{En} , is a common feature of all four form factors. It is striking how similar the contribution from the bump is in all four form factors. While it is only a small contribution to G_N^{std} , it dominates G_{en} at low momentum transfer where the contribution from the two dipoles, though both separately are large, cancel.

As also discussed in section 2, such bump structure in Q -space contributes a certain $\Delta\rho_b$ in r -space, the detailed structure of which, however, is not easy to foresee. The net charge in $\Delta\rho_b$ under discussion here is zero by construction, therefore it must show some oscillation. The wavelength λ_ρ of this oscillation is given by the position of the bump in Q -space, Q_b , as $\lambda_\rho = 2\pi\hbar/Q_b$. The damping of the oscillation is related to the relative width of the bump. From $Q_b \approx 0.45$ GeV/c = 2.3 fm⁻¹ there thus results the wavelength $\lambda_\rho = 2.7$ fm in agreement with the oscillation shown in fig. 2. We conclude that an oscillation with such wavelength results as a common feature from all four form factors and is not just a peculiarity of G_{En} .

We demonstrate this by showing in the following subsection the Fourier transforms of the four form factors.

4.3 The Fourier transform of the fits of the form factors

As mentioned above, the Fourier transforms of the Sachs form factors can be regarded as the charge and magnetic distribution, respectively, in the Breit frame. With this in mind we show in this subsection the Fourier transforms of the form factors which, for brevity, we all denote by “charge” ρ .

Fig. 6 shows $\rho(r)$ resulting from the two dipole contributions, the bump and their sum. For reference, the transform of the standard dipole is also shown. In this representation, for all three G_N^{std} $\rho(r)$ is very close to that of the standard dipole form for $r > 0.2$ fm. This is true for G_{Mp} also down to the centre of the nucleon, where we see deviations from the dipole form for G_{Ep} and G_{Mn} . It has to be admitted, however, that in the latter cases the measurements do not extend to as high Q^2 as in the former, thus the distribution in r -space is less well fixed at small r . Actually, there is only a tiny fraction of the total charge contained in this inner part. The contribution from the bump is not visible in this plot.

The quantity $\rho(r) \cdot r^2$ gives directly the weight of the charge contained in a spherical shell at distance r , thus the area under the curve gives the total charge contained in the respective term. This quantity is shown in fig. 7. Here, the contribution from the bump in the form factor is clearly visible as oscillation (net charge = 0). Its phase in r -space is such that it puts additional strength on the dipole form in the outer region with maxima between 1.5 (G_{Mp}) and 2.0 fm (G_{Ep} , G_{Mn}). The second dipole gives small and tiny contributions in the interior of $\rho(G_{Ep})$ and $\rho(G_{Mn})$, respectively, and is not visible in $\rho(G_{Mp})$. For G_{En} the oscillation gives the total $\rho(r)$ in the outer region centred around 1.7 fm, while the inner part is dominated by the difference of the two dipoles. In between there is a cancellation between these two terms, a feature already visible in the analysis in section 2. We come back to this point below.

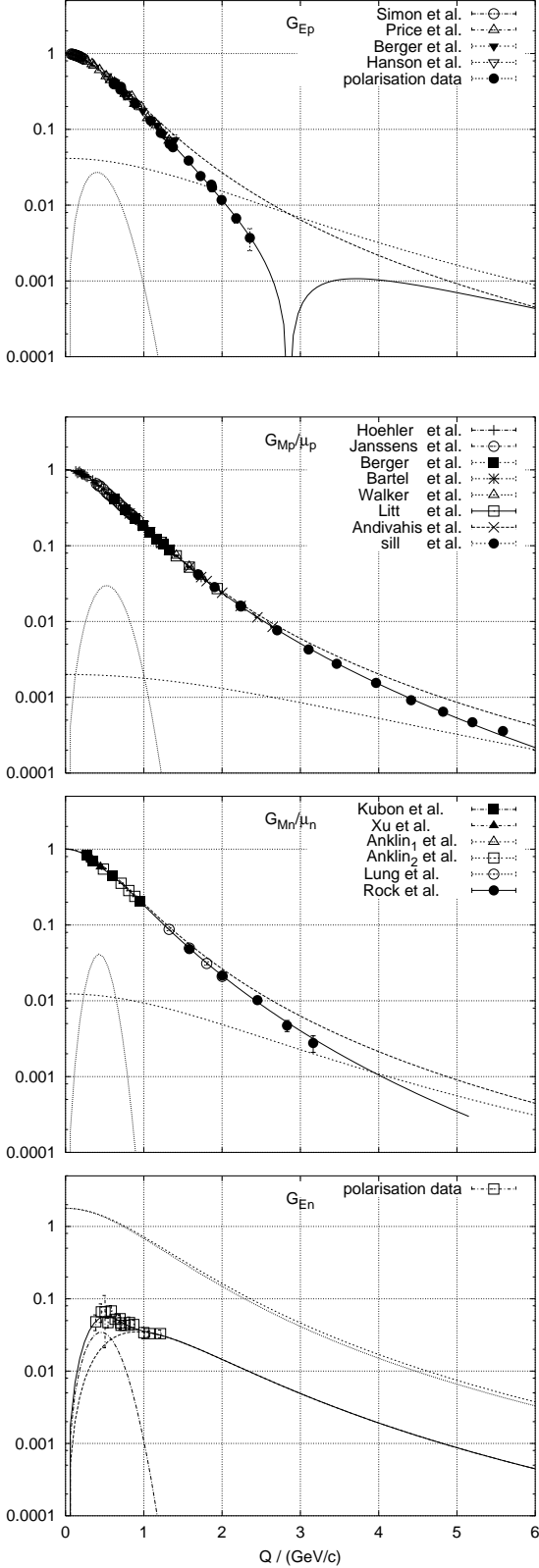


Fig. 3. The measured nucleon form factors and their description by the phenomenological fits. The full line represents the the sum of the two dipoles and the Gaussian, which are also shown separately, the second dipole form being multiplied by -1 in order to make it positive for this logarithmic plot. For G_{En} we also show the sum of the two dipoles separately.

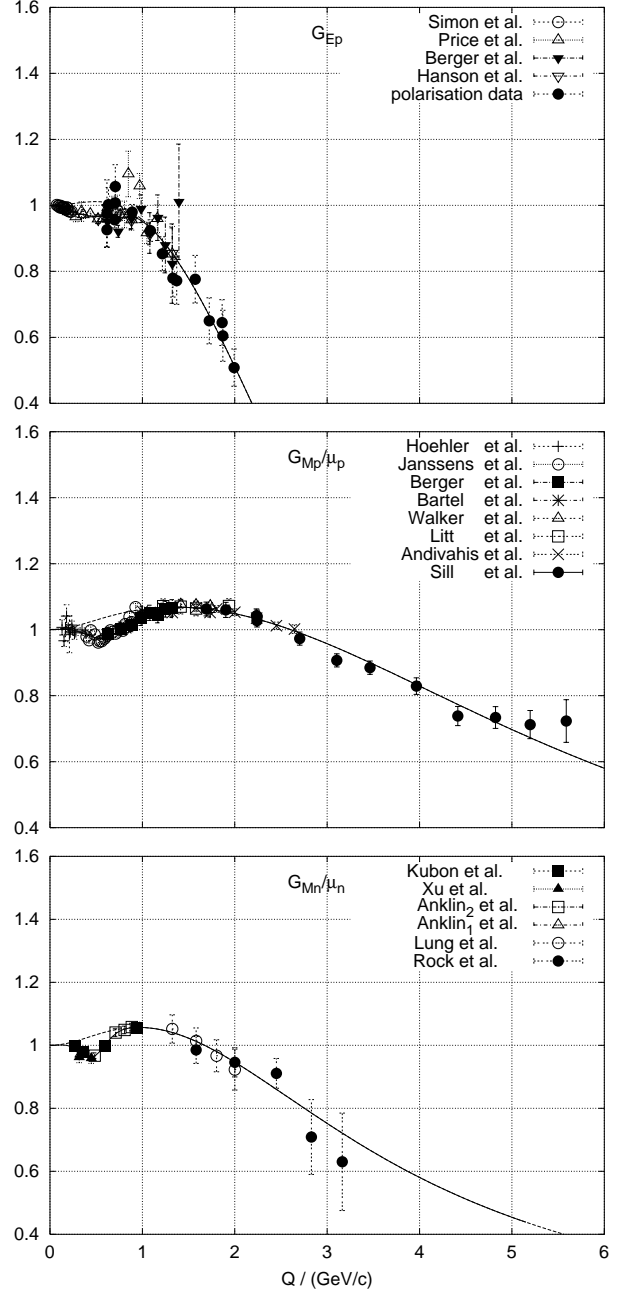


Fig. 4. The measured nucleon form factors and their phenomenological description divided by the standard dipole form factor. The full line represents the full fit, while the broken line is only the “smooth main part”, i. e. the sum of the two dipoles.

In order to emphasise the outer region of the nucleons even more, fig. 8 shows $|\rho(r)| \cdot r^2$ but now in a logarithmic scale. In this plot the sign information gets lost and one has to look at fig. 7 to keep track of the sign. The sign of the first lobe in the contribution $\Delta\rho_b(r)$ from the bump in the form factor, this means $a_b Q^2 G_b(Q)$, is that of $\Delta\rho_b(r = 0)$. Since $\Delta\rho_b(r = 0) \propto a_b \int G_b(Q) Q^2 dQ$, the sign of $\Delta\rho_b(r = 0)$ and thus the sign of the first lobe in $\Delta\rho_b(r)$ is given by the sign of the amplitude a_b of the bump ($G_b(Q) > 0$). - Here again, we do not want

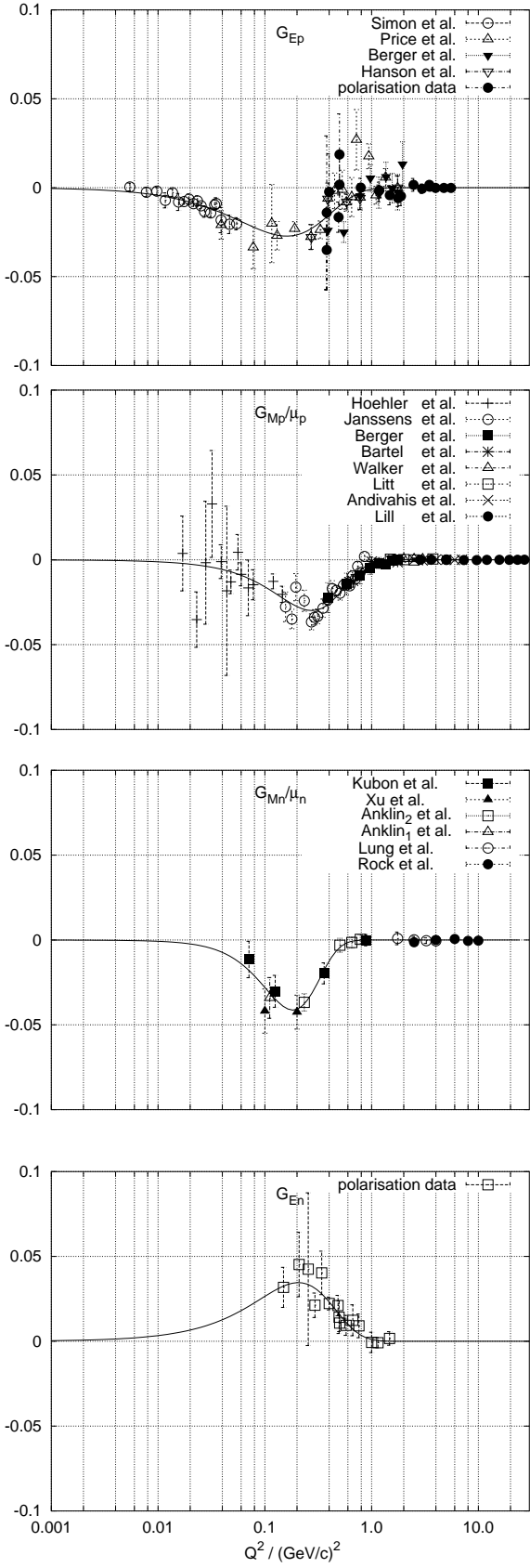


Fig. 5. The difference between measured nucleon form factors and the smooth part of the phenomenological ansatz with logarithmic x-scale for $Q^2 / (GeV/c)^2$.

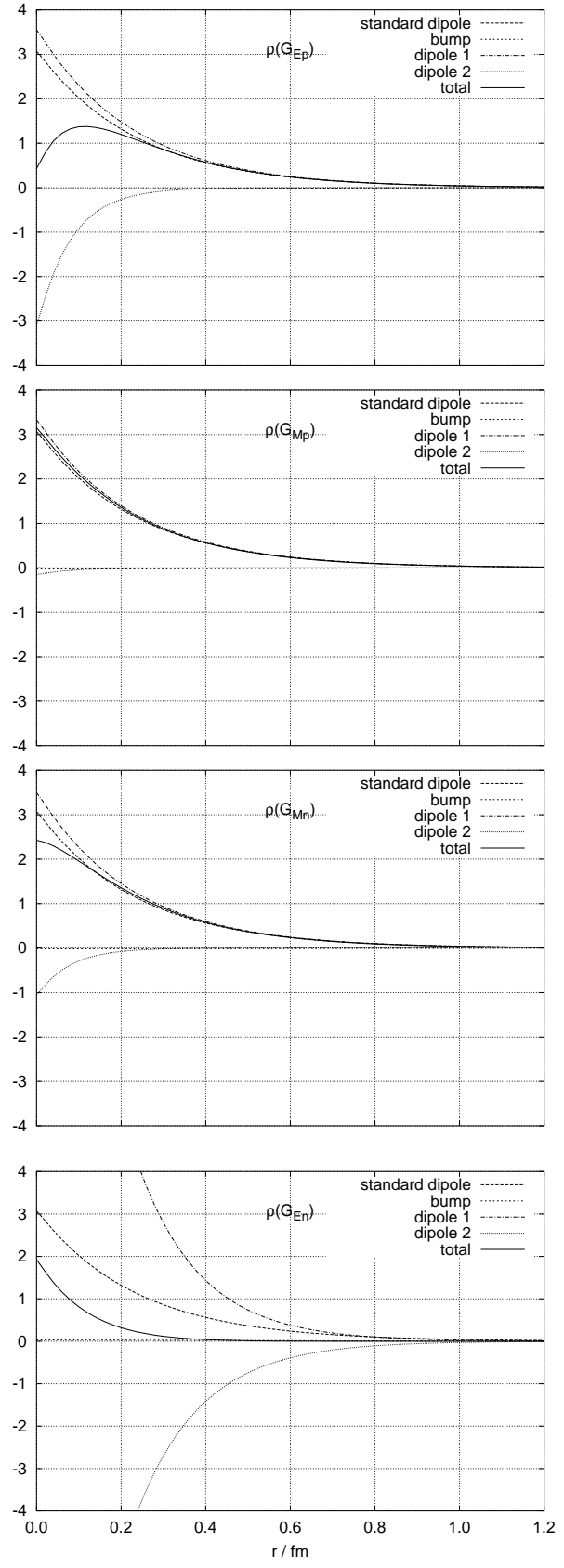


Fig. 6. $\rho(r)$ of the nucleons in the Breit frame. The units of $\rho(r)$ are fm^{-3} . The distributions are normalised to 1 for G_N^{std} and to 0 for G_{En} .

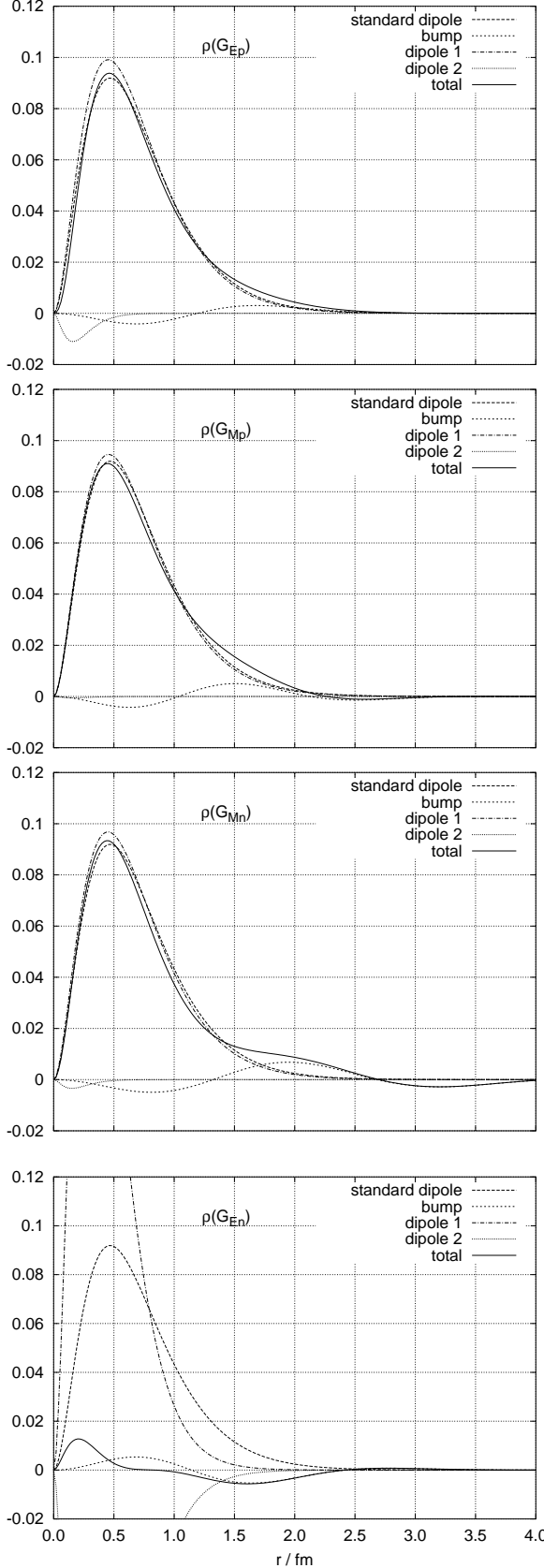


Fig. 7. $\rho(r) \cdot r^2$ in the Breit frame.

to go into details. We will see in the next section, that one \pm oscillation on top of a smooth distribution can be interpreted as dissociation of the nucleon in its counterpart and a pion cloud. The further oscillations visible in the logarithmic plot in fig. 8 are compatible with the data, but certainly must be regarded as depending on the special ansatz eq. (6).

5 A coherent description of the four form factors by a physically motivated ansatz

5.1 The ansatz

Inspired by the conspicuous graphical representation of the form factors, which reveal a bump on top of a smooth trend, we make the ansatz of describing the nucleons by the sum of a bare nucleon plus a polarisation part according to

$$p = a_p \cdot p^0 + b_p \cdot (n^0 + \pi^+) \\ = p^0 + b_p \cdot (-p^0 + n^0 + \pi^+), \quad (7)$$

$$n = a_n \cdot n^0 + b_n \cdot (p^0 + \pi^-) \\ = n^0 + b_n \cdot (+p^0 - n^0 + \pi^-) \quad (8)$$

where we have made use of the normalisation condition $a_N + b_N = 1$ for $N = p, n$. Neutral pions are not taken into consideration since, to first order, they do not contribute to elastic electron scattering.

The form factors can thus be written as

$$G_p = G_p^0 + b_p \cdot (-G_p^0 + G_p^0 + G^{\pi^+}) = G_p^0 + G_p^{pol}, \quad (9)$$

$$G_n = G_n^0 + b_n \cdot (+G_n^0 - G_n^0 + G^{\pi^-}) = G_n^0 + G_n^{pol} \quad (10)$$

where we use the transparent nomenclature of the form factor of the polarisation

$$G_N^{pol} = b_N \cdot (G_{\bar{N}}^0 - G_N^0 + G^{\pi}), \quad (11)$$

where \bar{N} denotes the neutron (proton) and π the π^+ (π^-) when N is the proton (neutron).

Furthermore, we think of the bare nucleons in terms of their constituent quark content, i. e. $p = (uud)$ and $n = (udd)$. We denote the form factor of the distribution of quark q in the nucleon N by G^{qN} . We are thus dealing with the ingredients G^{up} , G^{dp} , G^{un} , and G^{dn} for which we take the dipole form:

$$G^{qN} = \frac{a_0^{qN}}{(1 + Q^2/a_1^{qN})^2}. \quad (12)$$

The pion has intrinsic parity -1 which has to be compensated by its spatial wavefunction; therefore, to lowest order, it should be in an ($l=1$)-state. Taking as simple ansatz the wave function of a harmonic oscillator, the related form factor is given by

$$G^{\pi} = a_0^{\pi} \cdot (1 - \frac{1}{6}(Q/a_1^{\pi})^2) e^{-\frac{1}{4}(Q/a_1^{\pi})^2}. \quad (13)$$

The form factor of the pion cloud should be the convolution of this form factor from the wave function with that of the intrinsic distribution of the pion, the size of which is certainly not

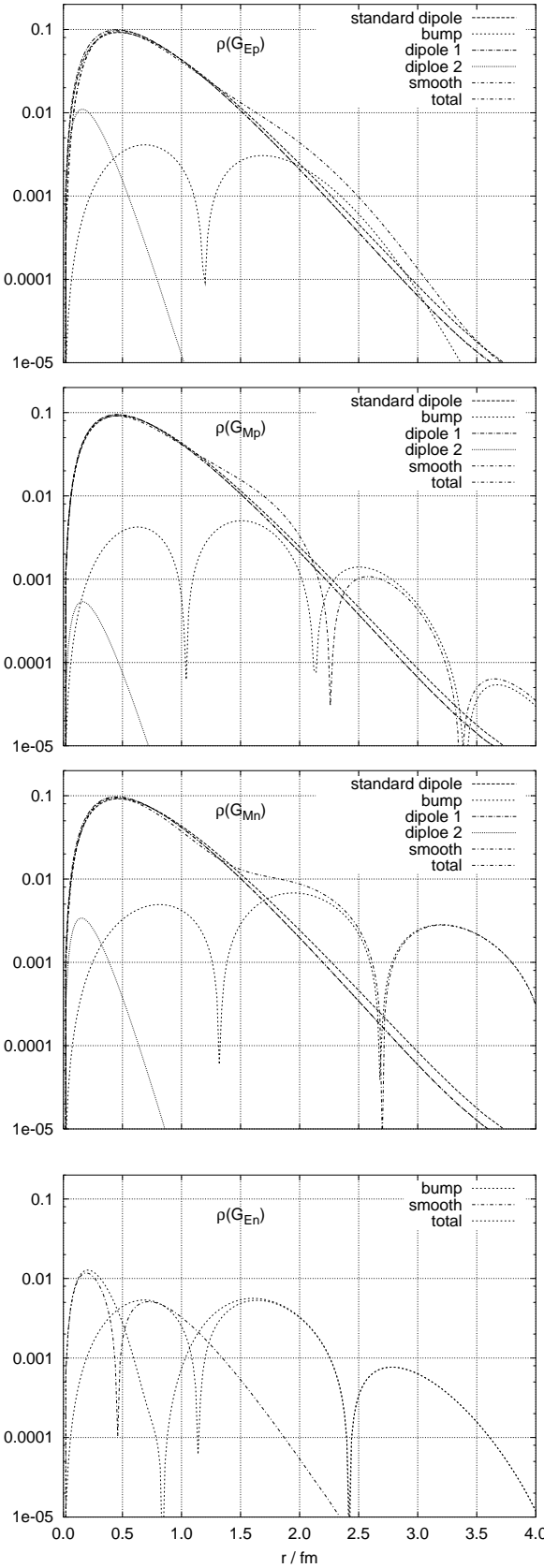


Fig. 8. $\rho(r) \cdot r^2$ in the Breit frame as in fig. 7, but now in a logarithmic scale.

negligible compared to that of the nucleon and thus to the extension of the pion cloud. Convolution in r -space results in a multiplication in Q -space. Assuming a Gaussian for the intrinsic pion distribution, this results in a multiplication of eq. (13) by a Gaussian, thus by a change of the parameter a_1^π in the exponential. This does not change the form of G^π , it would only decouple the parameter a_1^π in the exponential from that in the brackets. We will, however, not make use of this additional degree of freedom.

For the electric form factors, we have $a_{0,E}^{\pi^+} = -a_{0,E}^{\pi^-} = 1$. For the magnetic form factor, the situation is not that clear due to the degrees of freedom of the vector coupling of the magnetic moments. Furthermore, it is not clear what magnetic moment should be related with the pion cloud since we are not dealing with a free pion.

Strict isospin invariance would imply

$$\begin{aligned} G^{up} &\sim G^{dn}, \\ G^{dp} &\sim G^{un}, \\ G^{\pi^+} &\sim -G^{\pi^-}. \end{aligned} \quad (14)$$

We will check, whether the measured form factors can be described under this condition.

5.2 The electric form factors

Since $G_{En}^0(0) = 0$ due to the vanishing charge of the neutron, from eq. (9) we have

$$G_{Ep}(0) = [(1 - b_p) \cdot G_{Ep}^0(0) + b_p \cdot G_{\pi^+}(0)] = 1. \quad (15)$$

We note, that the charge $b_p \cdot 1$ of the pion cloud, which goes at the expense of the bare proton's charge, contributes to the proton electric form factor at $Q^2 = 0$. Therefore, the peak on top of a smooth part of the form factors, which we have revealed in section 4, cannot be attributed directly to the pion. In fact, to the contrary, according to eq. (13) the contribution from the pion cloud should be concentrated around $Q^2 = 0$ since the pion cloud is expected to extend further out than the bare proton.

According to our model, we evaluate the electric form factor of the proton with the ansatz

$$\begin{aligned} G_{Ep} &= (G_E^{up} + G_E^{dp}) \\ &+ b_p \cdot (-(G_E^{up} + G_E^{dp}) + (G_E^{un} + G_E^{dn}) + G_E^{\pi^+}) \end{aligned} \quad (16)$$

with G^{qN} and G^π parametrised by eqs. (12) and (13), respectively.

The weights a_0^{qN} for the electric quark form factors are given by the quark charges, i. e. $a_{0,E}^{up} = +4/3, a_{0,E}^{un} = +2/3$ and $a_{0,E}^{dp} = -1/3, a_{0,E}^{dn} = -2/3$, and that of the pion is $a_0^{\pi^+} = +1$. This ansatz conserves automatically the normalisation. We are thus left with the free parameters of the quark distributions, $a_1^{up}, a_1^{dp}, a_1^{un}, a_1^{dn}$, the amplitude b_p of the polarisation term and the oscillator parameter for the pion, $a_1^{\pi^+}$, i. e. we have one free parameter less than in the phenomenological model with two dipoles and the bump discussed in section 4.

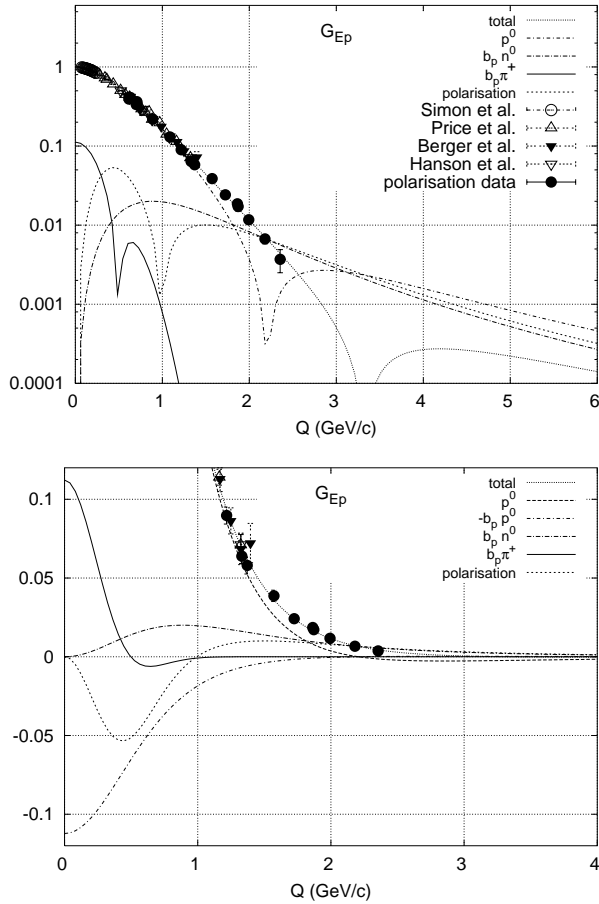


Fig. 9. G_{Ep} : Fit 2 (cf. table 3) compared to the measurements. Upper panel: Full scale comparison. Lower panel: The contributions to G_{Ep} in a linear scale for a discussion of the interplay of the different contributions to G^{pol} and, finally, the making up of G^{Ep} as the sum of G_p^0 and G^{pol} (note the extended x-scale in the lower panel). - The form factors of $p^0 + \pi^+$ are normalised to 1, that of n^0 to 0.

In a first fit we take these six parameters as free. The resulting values are given in table 3 as fit 1. It is not too surprising that the n^0 -parameters remain completely undetermined. The data are described by this ansatz as well as with the phenomenological ansatz with seven parameters ($\chi^2 = 59.6$ here compared to 59.7 there). We note that the pion parameters in this model are better determined than the bump parameters in the phenomenological ansatz. Further, the large values of a_1^{qn} would yield an extremely sharp localisation of the quarks in the neutron, most likely an unrealistic scenario. The large error on the neutron parameters, however, leave room for applying further model restrictions. In fit 2 we subject the quark distributions to complete isospin invariance, i. e. we demand $a_1^{un} = a_1^{dp}$ and $a_1^{dn} = a_1^{up}$, there are thus only 4 free parameters left. The proton parameters vary essentially only within their errors, the same is true for the pion-cloud parameters. The total χ^2 increases by the omission of the two parameters by only 1.5 which is an insignificant increase.

The fit 2 is compared in fig. 9 to the data. Here, we also show the single contributions of the model. In the logarithmic

plot (upper panel) their signs get lost, therefore, in order to discuss the interplay between the single contributions to G_{Ep} , we have plotted in the lower panel these contributions on a linear scale. The dominating G_p^0 from the bare proton p^0 has a zero around 2.2 GeV/c due to the interference between the positive G^{up} and the negative G^{dp} , the latter being suppressed by a factor 4, but extending out much further ($a_1^{dp} > a_1^{up}$; these contributions are not shown separately). This minimum, however, is shadowed by the polarisation term G_p^{pol} . At $Q^2 = 0$, $-b_p G_p^0$ and $b_p G_{\pi^+}^0$ cancel, while G_n^0 itself is zero there (see lower panel of fig. 9). With increasing Q , the negative contribution of $-b_p G_p^0$ prevails, G_p^{pol} thus becomes negative, until it is balanced by the positive contribution from the neutron, $b_p G_n^0$. Around $Q \approx 0.4$ GeV/c G_p^{pol} has a minimum, around $Q \approx 1.0$ GeV/c it passes through zero and becomes positive at large Q where the contribution $b_p G_n^0$ prevails. Finally there results a zero in G_{Ep} around 3.3 GeV/c due to the interference of the positive polarisation (from n^0) and the negative lobe of G_p^0 from its d -quark contribution. - The data are certainly not sufficient to fix these numbers precisely; nevertheless they are useful as a guidance for what might go on physically in this Q^2 -range. The determination of the minimum in G_{Ep} by experiment is highly desirable.

Comparison with the evaluation in terms of the purely phenomenological model in section 4 reveals that the bump structure there has a different meaning than that of the polarisation term resulting here from the evaluation in terms of the quark model. It is clear, that this is due to the definition of what is “bump” and what is “smooth”. The interpretation of this model, however, makes clear, that the low- Q^2 side of the bump results mainly from the interplay of the form factor from the π^+ with the reduction in p^0 .

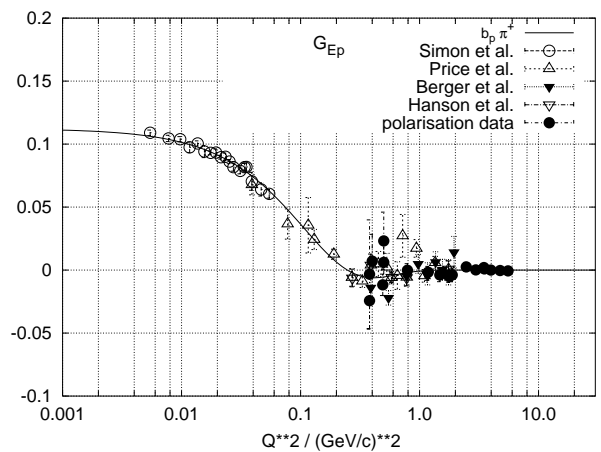


Fig. 10. The contribution $b_p G_E^{\pi^+}$ from the pion cloud to G_{Ep} (fit 2). For comparison the data points show the measurements $[(1 - b_p) \cdot G_{Ep}^0 + b_p \cdot G_{En}^0]$.

In fig. 10 we show on a logarithmic Q^2 -scale the contribution of the pion cloud for fit 2. This scale emphasises the low- Q^2 part, where the pion-cloud contribution is concentrated. It is obvious that the data are not precise enough to fix the zero

in $G_E^{\pi^+}$. A good determination of this zero, however, would be a prerequisite to distinguish between the parameter $a_1^{\pi^+}$ in the exponential and in the brackets, thus to see the signature of the finite size of the pion.

We have seen that in the fits to G_{Ep} the parameters of the contribution from G_n^0 remain practically undetermined. We now want to see what we learn about them from the electric form factor of the neutron, for which the corresponding expression is

$$G_{En} = (G_E^{un} + G_E^{dn}) + b_n \cdot ((G_E^{up} + G_E^{dp}) - (G_E^{un} + G_E^{dn}) + G_E^{\pi^-}). \quad (17)$$

As in the case of the proton, this ansatz conserves automatically the normalisation (here: to 0). Respecting strict isospin invariance, i. e. $a_1^{un} = a_1^{dp}$, $a_1^{dn} = a_1^{up}$, and $G_E^{\pi^+} = G_E^{\pi^-}$ we can calculate G_{En} from eq. (17). In the upper panel of fig. 11 we compare this calculation to the measured data, using the parameters of fit 2 for G_{Ep} . First, it is remarkable, that and how well the polarisation term, directly calculated with the parameters from the fit to G_{Ep} , reproduces the bump structure of G_{En} at low Q ! However, second, the contribution from the bare neutron alone, while being reasonably well positioned in Q , overestimates drastically the total measured G_{En} ,

There are two ways to reduce the amplitude of the superposition of two dipoles with equal amplitudes of different sign. The first way is to just reduce the common amplitude, here one would need a reduction of roughly a factor of 6. The amplitude being given by the charge of the one *up* and the two *down* quarks as $+2/3$ and $-2/3$, respectively, such reduction would mean to leave the grounds of the present model, namely the building up of the nucleons by constituent quarks. Therefore, we prefer the second way which requests letting the two parameters a_1^{un} and a_1^{dn} approach each other. In the fit we let the routine search for an appropriate parameter choice by varying only a_1^{un} , a_1^{dn} , and b_p . In fact, the program finds a perfect fit to the measured G_{En} with a χ^2 per d. f. of 0.87 (fit 2). While fit 2 reduces the polarisation term by only some 20 %, the dipole parameters are increased by a factor of 5 and 2, respectively, which corresponds to making the distribution in r -space very narrow. Furthermore, $a_1^{un}/a_1^{dn} = 1.2$ whereas $a_1^{dp}/a_1^{up} = 2.5$, i. e. the *up*- and *down*-quark distributions are much more similar in n^0 than in p^0 . This finding, however, may not be too surprising since at the small distances of fractions of a *fm* the difference in the Coulomb interaction in p^0 and n^0 might make strict isospin symmetry questionable. In other words, the net positive charge of the two up constituent quarks will repel them so they reside more outside than the quarks with the net zero charge in the neutron. One should not mix this up with the opposite behaviour of the current quark distribution as derived from deep inelastic scattering. - The result of this fit is shown in the middle panel of fig. 11.

In a last step (fit 3) we examine the significance of the fit of a_1^{un} and a_1^{dn} by setting a_1^{un} equal to a_1^{dp} from fit 2 of G_{Ep} and keeping this fixed. We thus allow only a_1^{dn} and b_n to vary. While the resulting b_n differs by less than one standard deviation from its value in fit 2, a_1^{dn} just follows a_1^{un} in order to keep the difference small, which, as said above, is necessary to keep the G_{En} small in the high- Q region. As expected from

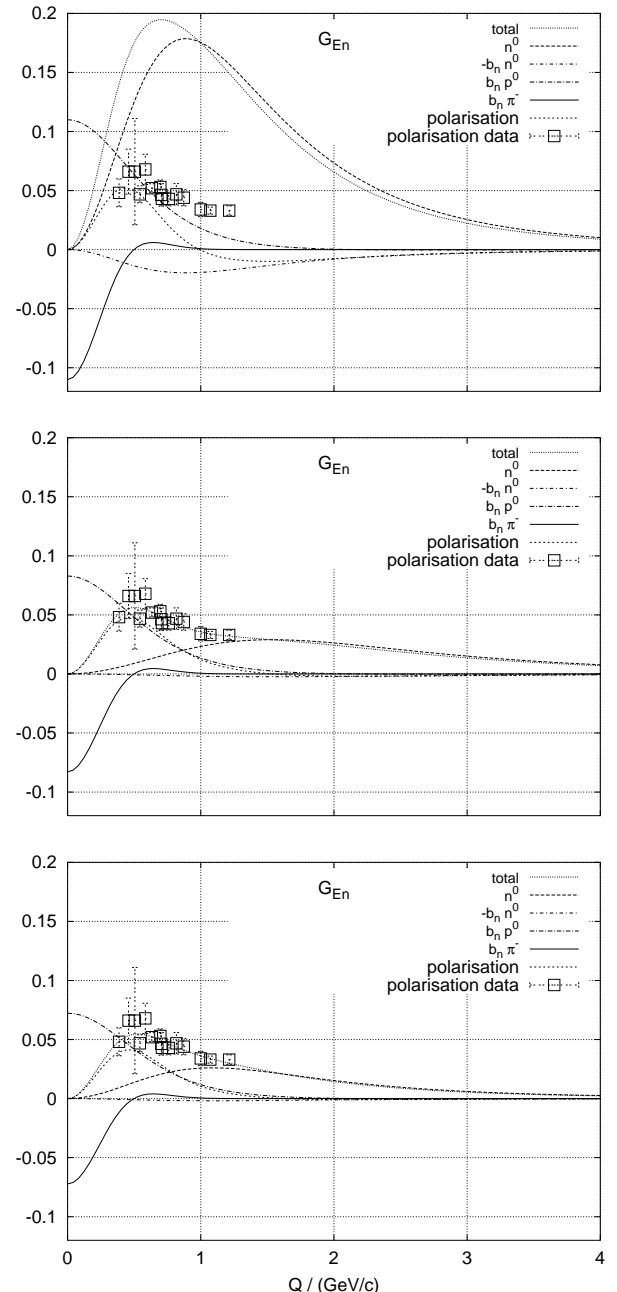


Fig. 11. G_{En} : Calculation with eq. (17) compared to the measurements. Upper panel: Calculation obeying strict isospin invariance. Middle panel: a_1^{un} , a_1^{dn} , and b_p fitted to the G_{En} -data (see fit 2 to G_{En} in table 3). Lower panel: a_1^{dn} and b_n fitted to the data (see fit 3 to G_{En} in table 3).

the large uncertainties in a_1^{un} and a_1^{dn} in fit 2, χ^2 only varies by 0.8 with this quite drastic variation in a_1^{un} . The result of this fit is shown in the lower panel of fig. 11.

Data at higher momentum transfers are needed to further constrain the low-distance behaviour of the neutron form factor.

We have checked the significance of the bump-structure in G_{En} by fitting the data with only a smooth ansatz consisting

form factor	G_p^0		G_n^0		G^{π^+}		$N_{d.f.}$	$\chi_{d.f.}^2$	χ_{total}^2
	a_1^{up} (GeV/c)**2	a_1^{dp} (GeV/c)**2	a_1^{un} (GeV/c)**2	a_1^{dn} (GeV/c)**2	$b_{p,n}$	$a_1^{\pi^{+/-}}$ GeV/c			
G_{Ep}									
1	1.000(100)	2.03(72)	57.(1200.)	78.(2500.)	0.10(4)	0.198(12)	64	0.932	59.6
2	1.008(20)	2.54(16)	2.54(-)	1.008(-)	0.11(1)	0.203(6)	66	0.926	61.1
3	1.051(20)	2.391(14)	2.53(-)	2.22(-)	0.118(13)	0.204(6)	66	0.928	61.2
G_{En}									
1	1.008(-)	2.54(-)	2.54(-)	1.008(-)	0.11(-)	0.203(-)	-	-	-
2	1.008(-)	2.54(-)	5.1(4.8)	4.4(4.0)	0.083(11)	0.203(-)	12	0.871	10.5
3	1.008(-)	2.54(-)	2.54(-)	2.22(3)	0.072(6)	0.203(-)	13	0.865	11.3

Table 3. Parameters from the fits of the model ansatz to the electric nucleon form factors. For the error convention see caption of table 2. The different fits observe more or less to isospin symmetry (see text).

form factor	outer distr.		inner distr.		G^{π}		$N_{d.f.}$	$\chi_{d.f.}^2$	χ_{total}^2
	a_0^{out}	a_1^{out} (Gev/c) ²	a_0^{in}	a_1^{in} (Gev/c) ²	$a_0^{\pi^{+/-}}$	$a_1^{\pi^{+/-}}$ (Gev/c)			
G_{Mp}/μ_p									
1	0.914(5)	0.818(8)	-0.0049(1)	9.578(1.2)	0.110(7)	0.213(7)	75	0.887	66.5
2	0.917(6)	0.811(16)	-0.0034(14)	13.57(6.0)	0.106(8)	0.210(8)	69	0.901	62.2
G_{Mn}/μ_n									
1	1.019(14)	0.939(110)	-0.112(16)	2.37(1.1)	0.219(47)	0.152(9)	14	0.629	8.8
2	1.363(3.14)	1.173(700)	-0.511(3.17)	1.789(2.0)	0.140(46)	0.213(-)	15	0.946	14.9
3	1.189(1.34)	1.060(460)	-0.309(1.38)	1.853(1.8)	0.120(40)	0.189(19)	15	0.837	12.6

Table 4. Parameters for the fits to the magnetic form factors. In all but fit 3 for G_{Mn} the normalisation is free. G_{Mp} ($Q_{max}^2 = 31.2$ (GeV/c)²): Fit 1: Fit to all data, all parameters free. Fit 2: Fit to the data up to 10 (GeV/c)² with all parameters free. G_{Mn} ($Q_{max}^2 = 10$ (GeV/c)²): Fit 1: All parameters free. Fit 2: $a_1^{\pi^-}$ kept fixed at 0.213 (GeV/c) as determined for G_{Mp} . Fit 3: Normalisation kept fixed by adding a point with value 1.0000 ± 0.0001 at $Q^2 = 0$.

of two dipoles with equal but opposite amplitudes, which is equivalent to the ansatz eq. (1). With this parametrization we get $\chi_{total}^2 = 11.5$ (*d.f.* = 12), i. e. an increase by 1.0 compared to fit 2 in table 3. Thus, for a significant determination of the bump more precise data at low Q^2 are needed as well as data extending to higher Q^2 .

Finally, we check whether the fit of the proton's electric form factor is deteriorated when the neutron parameters are kept fixed to the values determined now from the fit to the neutron data. The resulting parameters are shown as fit 3 of G_{Ep} in table 3. In fact the change in the parameters and thus also in the graphical representation of the form factor are so small that we need not go into any detail here.

Summarising up for the electric form factors, G_{Ep} and G_{En} can be described on the same footing by our constituent-quark-pion ansatz.

5.3 The magnetic form factors

For G_{Mp} data are measured up to $Q^2 = 30$ (GeV/c)², therefore in this respect the situation is more favorable here. On the other side, the interpretation of the magnetic form factor within our model is hampered by the additional degree of freedom of the vector coupling of the spins and the magnetic moments: While it is clear, that, e. g., the two *u*-quarks in the proton carry the charge $2 \cdot 2/3$, the resulting magnetic moment depends on the coupling of the quark spins. Furthermore, it is not clear what magnetic moment one has to attribute to the constituent quarks. The same uncertainty holds for the contribution of the pion. Though it should predominantly be in a *p*-state, the related magnetic moment is not known, since the pion is highly off-mass shell and therefore its mass is not that of the free pion. Furthermore, its contribution to the total magnetic moment depends on the vector coupling. Therefore, in the evaluation of the magnetic form factors with the ansatz eqs. (16,17) with

eqs. (12,13) we have to take also the amplitudes a_0^{qN} and a_0^π as free parameters.

On the other side, one might think that the parameters a_1^{qN} , which describe the spatial distributions, might be the same for G_M and G_E such that they can be taken from there. One could, however, only profit from this for the sufficiently well determined bare proton part, and here only for the dominating term from the u -quarks. However, it is not clear whether the dipole parameter, determined at relatively low Q^2 , really should hold up to the highest Q^2 to which G_{Mp} has been measured. Furthermore, the magnetic operator does not weight the distribution in the same way as does the electric operator. Therefore, also the parameters a_1^{qN} have to be taken as free.

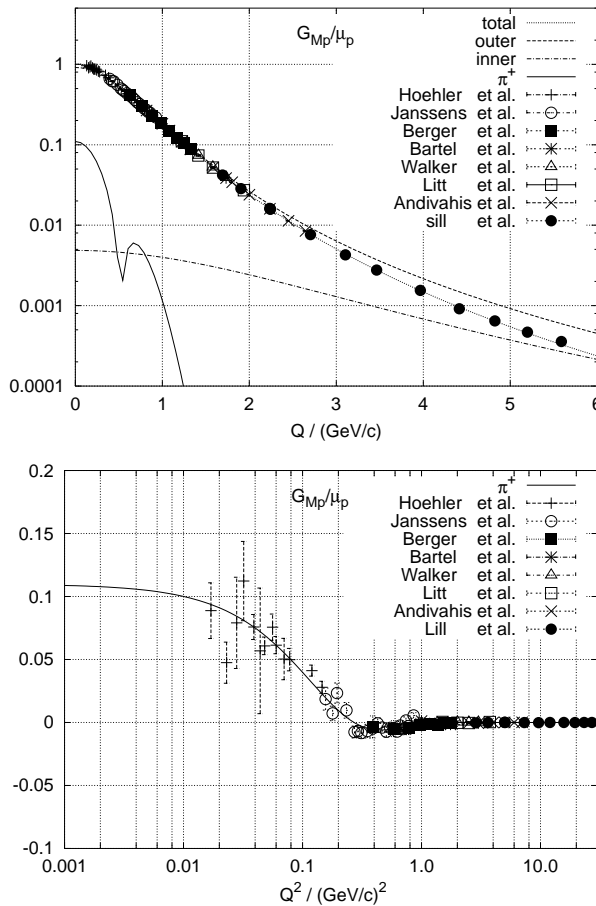


Fig. 12. The magnetic form factor of the proton (parameters from fit 1). Upper pannel: Comparison of the measured data with $G^{out} + G^{in} + G\pi^+$ (total) and the three contributions to the fit separately. Lower pannel: The data points show the measurements $-[G^{out} + G^{in}]$, compared to the pion cloud $a_0^{\pi^+} \cdot G^{\pi^+}$. Note that here the data are shown as function of $\log(Q^2)$ in order to emphasize the low- Q^2 region.

Isospin symmetry would suggest that there are only two different distributions, that for u - and d -quark in the proton, and in the neutron, respectively, the inverted case. In this case, including the pion there are only three distributions left and we try the ansatz

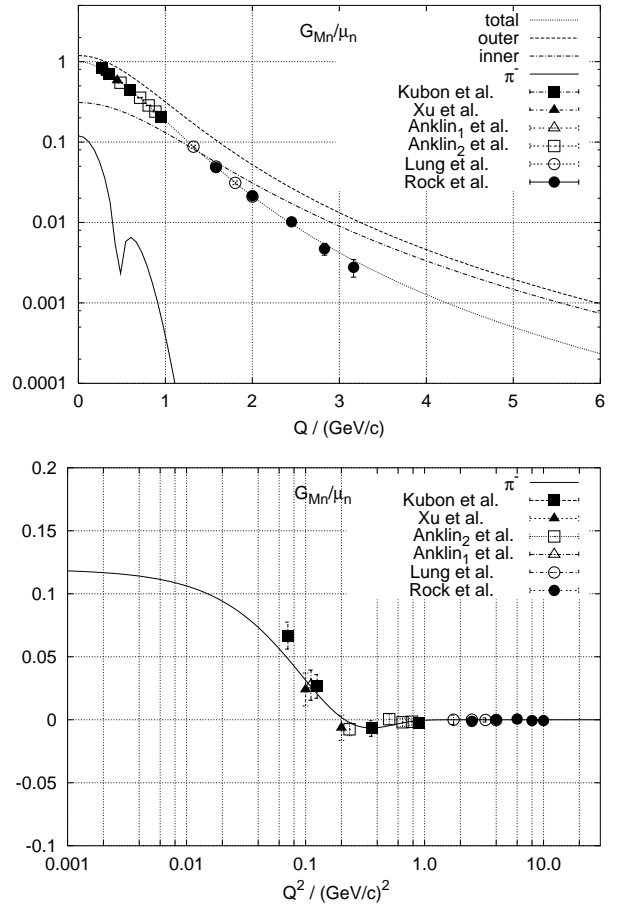


Fig. 13. Same as fig.12, now for G_{Mn} ; fit 3 in table 4.

$$G_M = a_0^{out} \cdot G^{out} + a_0^{in} \cdot G^{in} + a_0^\pi \cdot G^\pi. \quad (18)$$

Here, the nomenclature reminds on *inner* and *outer* quarks, and we omit any discussion about the coupling of their magnetic moments by just giving free amplitudes $a_0^{out,in}$ to their respective contributions to the magnetic form factors which, again, are parametrized by the dipole form eq. (12) with the free parameters $a_1^{out,in}$. In the same way we allow for a free amplitude for the pion cloud. With the a_0 as free parameters, normalization is not guaranteed. - We only mention in passing, that we have checked fits with three dipoles; even in the case of G_{Mp} , however, up to the highest Q^2 two dipoles are sufficient.

The parameters from the fits are tabulated in table 4. In the fits 1, all 6 parameters of the ansatz were free. Again χ^2 is comparable to the data evaluation with the phenomenological ansatz. We show in the upper panels of figs. 12 and 13 how well the data are described. Here, the three terms are also shown separately.

For G_{Mp} we find a surprisingly large value for a_1^{in} , corresponding to a concentration of the respective distribution in r -space near the origin (see subsection 5.4 below), however with very small amplitude. For the sake of comparison with G_{Mn} , we have repeated the fit with restricting the data to the Q^2 -range for which there are data for both magnetic form fac-

tors (fit 2). We find such large values for $a_1^{in}(G_{Mp})$ also from this restricted data base. About 90% of the (positive) magnetic moment of the proton is carried by the *outer* distribution ($a_0^{out}(G_{Mp}) \approx 0.91$) and 10% by the pion cloud ($a_0^{\pi^+}(G_{Mp}) \approx 0.11$). Note, that the normalisation is violated by some 2%. This should be acceptable in view of the quality of the data at low Q^2 . The *inner* distribution contributes only about -0.4% to the magnetic moment, while its contribution to the form factor becomes comparable at large Q^2 . Further, $a_1^{out}(G_{Mp})$ is 20% smaller than $a_1^{up}(G_{Ep})$, thus the related distribution in r -space extends further out for the magnetism than for the charge.

In fit 1 of G_{Mn} , the dominant contribution to the magnetic moment again comes from the *outer* distribution (note that by referring to G_{Mn}/μ_n the signs are inverted). The sign of the *inner* distribution again is negative, in this case, however, its contribution to the magnetic moment is about 11% and thus not negligible. The pion cloud contributes a factor of two more to μ_n than to μ_p in this fit. It has to be admitted, however, that in this fit the normalisation is off by about 10%. In fact, the data do not extend sufficiently far down in Q^2 to let the normalisation free in the fit, and the pion cloud is particularly sensitive to the data at low Q^2 . Fit 2 shows the result of a fit with $a_1^{\pi^-}(G_{Mn})$ fixed to $a_1^{\pi^+}(G_{Mp}) = 0.213$ GeV/c. The fit now obeys normalisation to within a percent with the amplitudes a_0^{out} and a_0^{in} having very large (correlated!) errors. With fit 3 we went one step further by adding an additional data point at $Q^2 = 0$ in order to fix the normalisation, while at the same time letting the parameter $a_1^{\pi^-}(G_{Mn})$ free. There is some redistribution between *inner* and *outer* distribution, but all changes of the parameters are within the errors. Thus, there is no problem with the normalisation of the data. - We only mention in passing that taking into account also the data by Markowitz et al. [39] and by Bruins et al. [40] yield $a_0^{\pi^-}(G_{Mn})$ between 0.09 and 0.12 and $a_1^{\pi^-}(G_{Mn})$ between 0.186 and 0.189 GeV/c.

It is beyond the scope of this analysis to try an explanation of these findings.

5.4 The distributions in r -space

In fig. 14 we again show the distributions $r^2 \cdot \rho(r)$ in the Breit frame for the three standard form factors, now for the model evaluation calculated with parameters given in tables 3 and 4. In the proton, the contribution from the *inner* distribution is practically invisible. This shows that, to the degree of precision visible in this plot, the proton form factors are describable by one dipole plus the contribution from the π^+ , which builds a shoulder on the distribution extending out beyond 2 fm. The magnetic distribution in the neutron has an appreciable contribution from the *inner* distribution. Note that by evaluating G_{Mn}/μ_n all signs are inverted such that, e. g., the contribution from the π^- comes in with a positive sign. It is worth to mention, however, that it is the fit which yields the positive sign for the contribution parametrised as form factor of a 1p wave function.

To emphasize again the smaller contributions and thus in particular the outer region, fig. 15 shows $r^2 \cdot \rho(r)$ in logarithmic scale. By construction, the distinct structure at the edge

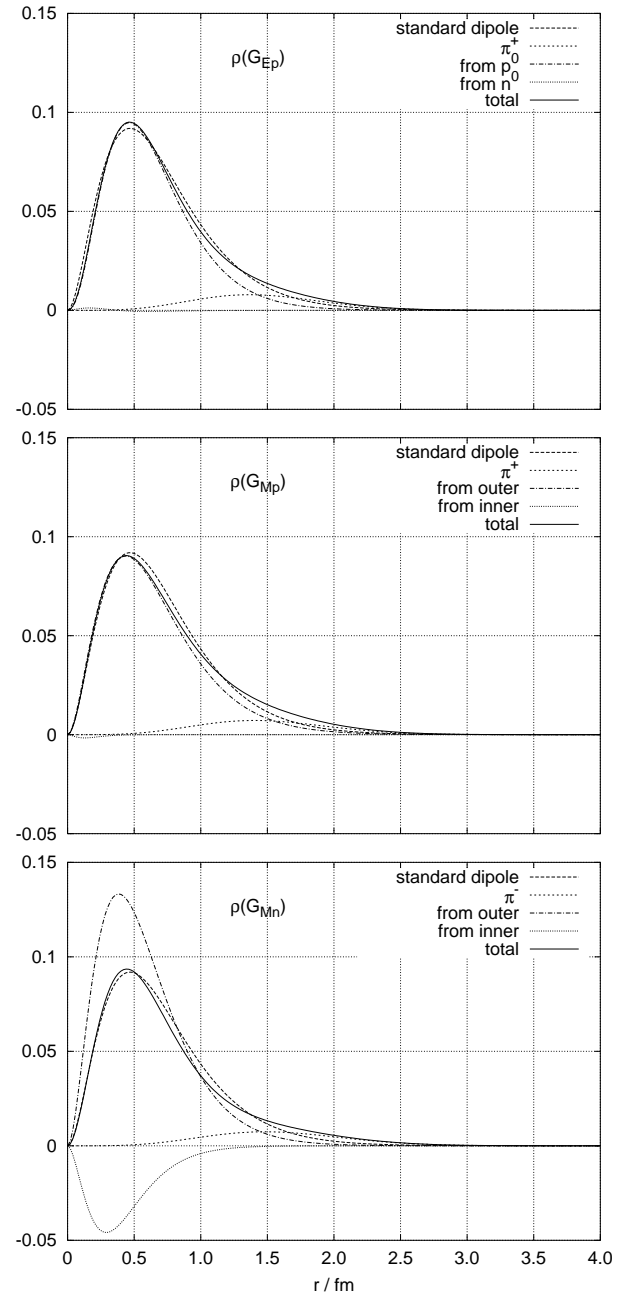


Fig. 14. $r^2 \cdot \rho(r)$ in the Breit frame, calculated with parameters given in tables 3 and 4 (G_{Ep} : Fit 3, G_{Mp} : Fit 2, G_{Mn} : Fit 3).

of the distribution now consists of only one bump, which, according to the model, is due to the pion cloud. This evaluation shows that the oscillations in the phenomenological analysis in section 4 are not significantly determined by the data, they result from the particular phenomenological ansatz used there for the separation between a “smooth” and a “bump” contribution to the form factor. The shoulders in all three standard form factors, however, emerge in both evaluations, and we judge them as being an unambiguous result from the data.

In fig. 16 we show the polarisation contributions to the electric form factor of the proton in an enlarged scale for a closer

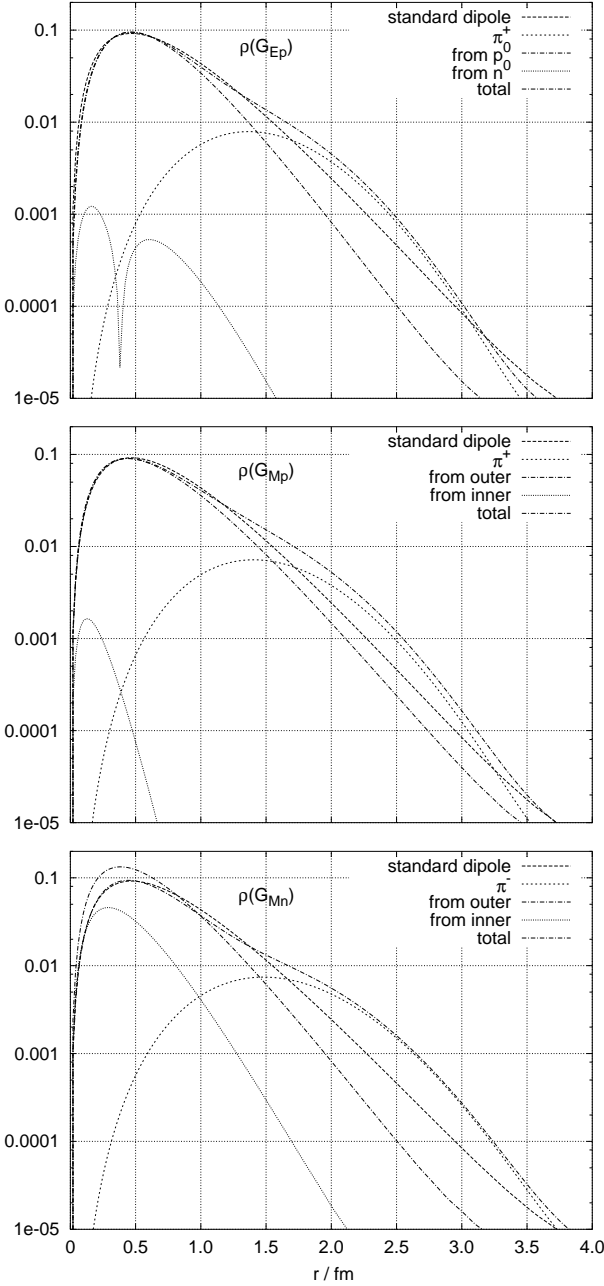


Fig. 15. Same as fig. 14, now in logarithmic scale.

comparison with the situation in the neutron which is shown in fig. 17. The (tiny) neutron contribution to the polarisation part of the proton, $b_p \cdot n^0$, is situated in the inner region. The superposition of $-b_p \cdot p^0$, i. e. from the reduction of p^0 , and $b_p \cdot \pi^+$ yields just the two lobes which were also seen in the phenomenological analysis and which are emphasized in the logarithmic representation in fig. 8. The small shift in the zero compared to fig. 8 is due to the difference in what is regarded as the smooth part of the form factor. In fig. 15 the negative lobe of the “bump” in fig. 8 is not visible since $-b_p \cdot p^0$ is absorbed in the contribution from p^0 as a whole.

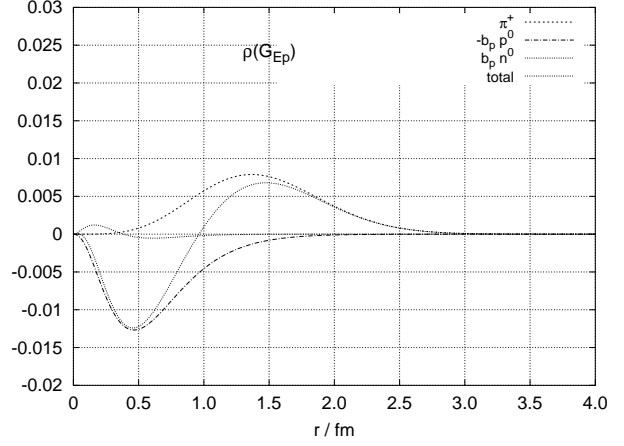


Fig. 16. The contribution of the polarisation term to $r^2 \cdot \rho(r)$ for the proton (in the Breit frame).

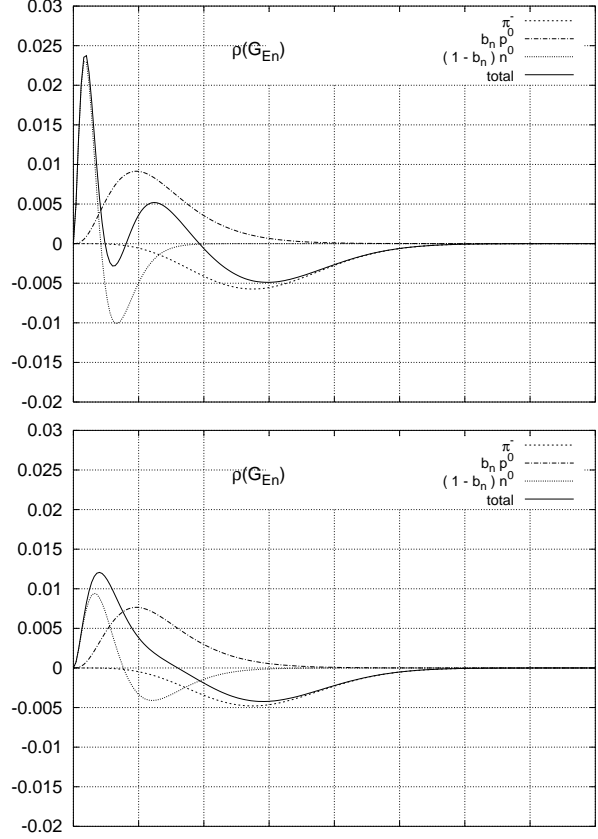


Fig. 17. $r^2 \cdot \rho(r)$ in the neutron (in the Breit frame). The contributions from the bare neutron and proton and from the pion are shown separately. Upper panel: Fit 2, lower panel: Fit 3 in table 3.

The charge distribution of the neutron, see fig. 17, is dominated by the smooth polarisation oscillation, i. e. by the positive lobe $b_n \cdot p^0$ and the negative lobe from the π^- . These two contributions add up to the same form as the polarisation in the proton, but with opposite sign. Superimposed is now the charge distribution from the neutron, $(1 - b_n) \cdot n^0$, which modifies the smooth oscillation in a characteristic way. In particular it reduces the positive lobe from $b_n \cdot p^0$ around 0.5 fm, possibly leading to a region with zero net charge. The details depend on differences in the ansatz, the present data do not contain sufficient information to discriminate between the different solutions. It is, however, gratifying to note that this feature is present throughout the different approaches in this paper: It is also visible in figs. 2 and, particularly clearly, in the lowest panel of fig. 7.

6 Conclusion

It is found as a common feature of all four nucleon form factors that they exhibit a very similar structure at small momentum transfer, which is related with some structure in r -space at large r around 2 fm. Such finding asks for a common explanation. We propose to interpret this as resulting from a pion cloud around the bare nucleon. A fit of the data with the ansatz of a p-wave for the pion yields probabilities for the dissociation of the nucleons into their counter part and a charged pion of 7 to 20%, details being dependent on peculiarities of the ansatz. This exciting result shows that further studies at momentum transfer $Q^2 \lesssim 1 \text{ (GeV/c)}^2$ and down to the lowest reachable values are much needed with increased precision.

We have parametrised the smooth part of the form factors by the superposition of dipoles, which lend themselves to an interpretation in terms of the distribution of constituent quarks. Data at high momentum transfers are needed to constrain these distributions.

The authors are indebted to M. Seimetz and D. Glazier for making available their G_{En} -measurements prior to publication. A careful reading of the manuscript by Dr. U. Mueller is gratefully acknowledged.

This work was supported by the state of Rhineland-Palatinate and by the Deutsche Forschungsgemeinschaft (SFB 443).

References

1. T. Eden *et al.*, Phys. Rev. **C 50** (1994) 1749.
2. M. Ostrick *et al.*, Phys. Rev. Lett. **83** (1999) 276.
3. C. Herberg *et al.*, Eur. Phys. J. **A 5** (1999) 131.
4. I. Passchier *et al.*, Phys. Rev. Lett. **82** (1999) 4988.
5. D. Rohe *et al.*, Phys. Rev. Lett. **83** (1999) 4257.
6. J. Becker *et al.*, Eur. Phys. J. **A 6** (1999) 329.
7. J. Bermuth, PhD Thesis, University of Mainz, 2001, publication in preparation
8. J. Golak *et al.*, Phys. Rev. **C63** (2001) 034006
9. H. Zhu *et al.*, Phys. Rev. Lett. **87** (2001) 081801.
10. M. Seimetz, PhD Thesis, University of Mainz, 2003 and to be published
11. D. Glazier, PhD Thesis, University of Glasgow, 2003 and to be published
12. D. Madey, Electron-Nucleus Scattering VII Conference, Elba International Physics Center, June 24-28, 2002, Proceedings to appear in EPJ A
13. T. Reichelt, International Conference "Quark and Nuclear Physics 2002 (QNP2002)", Forschungszentrum Juelich, Germany, June 9-14, 2002, Proceedings to appear in EPJ A
14. D. Day, see ref. [12]
15. S. Kopecky *et al.* Phys. Rev. **C56** (1997) 2220
16. F. Halsen and A. D. Martin, "Quarks and Leptons" (1984) John Wiley & Sons, Inc., New York
17. N. Isgur, Phys. Rev. Lett. **83** (1999) 272.
18. J. J. Kelly, arXiv:hep-ph/0204239.
19. G.G. Simon *et al.* Nucl. Phys. **A333** (1980) 381.
20. L.E. Price *et al.* Phys. Rev. **D4** (1971) 45.
21. Ch. Berger *et al.* Phys. Lett. **35B** (1971) 87
22. L. Andivahis *et al.*, Phys. Rev. D **50** (1994) 5491.
23. K.M. Hanson *et al.* Phys. Rev. **D8** (1973) 753
24. Th. Pospischil *et al.* Eur. Phys. J. **A 12** (2001) 125
25. B.D. Milbrath *et al.* Phys. Rev. Lett. **82** (1999) 2221
26. S. Dieterich *et al.* Phys. Lett. **B 500** (2001) 47
27. M.K. Jones *et al.* Phys. Rev. Lett. **84** (2000) 1398
28. O. Gayou *et al.* [Jefferson Lab Hall A Collaboration], Phys. Rev. Lett. **88** (2002) 092301.
29. G. Hoehler *et al.* Nucl. Phys. **B114** (1976) 505
30. T. Jannssens *et al.* Phys. Rev. **142** (1966) 922
31. W. Bartel *et al.* Nucl. Phys. **B58** (1973) 429
32. R.C. Walker *et al.* Phys. Rev. **D49** (1994) 5671
33. J. Litt *et al.* Phys. Lett. **B31** (1970) 40
34. A.F. Sill *et al.* Phys. Rev. **D48** (1993) 29
35. A. Lung *et al.* Phys. Rev. Lett. **70** (1993) 718
36. G. Kubon *et al.* Phys. Lett. **B524** (2002) 26
37. W. Xu *et al.* Phys. Rev. Lett. **85** (2000) 2900
38. H. Anklin *et al.* Phys. Lett. **B336** (1994) 313
39. P. Markowitz *et al.* Phys. Rev. **C48** (1993) R5
40. E.E.W. Bruins *et al.* Phys. Rev. Lett. **75** (1995) 21
41. J. Jourdan *et al.* Phys. Rev. Lett. **79** (1997) 5186
42. E.E.W. Bruins *et al.* Phys. Rev. Lett. **79** (1997) 5187
43. H. Anklin *et al.* Phys. Lett. **B428** (1998) 248
44. S. Rock *et al.* Phys. Rev. Lett. **49** (1982) 1139
45. E.J. Brash *et al.* Phys. Rev. **C65** (2002) 051001(R)
46. D.H. Perkins, Introduction to high energy physics, Addison-Wesley Publishing Company 1987
47. I. Sick Nucl. Phys. **A218** (1974) 509